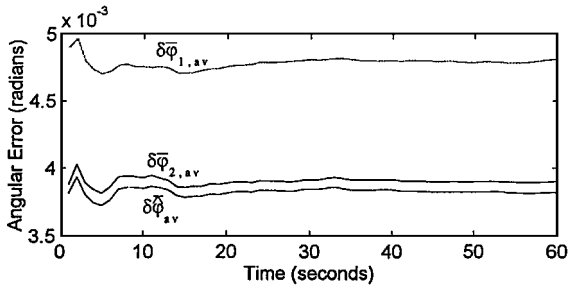

Fig. 5 Running time average of the ensemble average of the error associated with A_1, A_2, and $\hat{A}$ for a time-varying A_{true}.

Because the idea behind this algorithm is borrowed from linear estimation theory of independent unbiased measurement errors, one would expect the ensemble average of the angular error to be zero; however, as can be seen in Figs. 2 and 4, this is not the case. This discrepancy stems from the fact that the displayed error is not linearly related to the averaged matrices. Also, the errors in the computed matrices A_1 and A_2 are not really independent.

Finally, the vectors v_1 and v_2, which are the components of the two abstract vectors resolved in the reference coordinates, were constant through all runs, and the angle between the two vectors was close to 90 deg. To investigate the behavior of the algorithm for a different separation angle, we chose two new v_1 and v_2 vectors with a separation angle close to 45 deg and performed the dynamic test case. The results were similar to those presented in Figs. 4 and 5; however, the errors of all three algorithms were nearly 25% higher, as expected.

IV. Conclusions

We have presented a simple TRIAD-based algorithm, which we call Optimized TRIAD, that consistently outperformed TRIAD in simulated studies. The algorithm consists of solving TRIAD twice, once with one vector as the anchor and once with the other vector as the anchor, weight averaging the two resultant matrices, and orthogonalizing the final matrix. The weights are determined by the statistics of the measuring devices that produced the vector measurements. The idea behind this algorithm is borrowed from linear estimation theory of independent unbiased measurement errors. However, although the blending of the two TRIAD-generated matrices is based on an unbiased minimum variance formula, the ensemble average of the angular error is not zero because the error is not linearly related to the averaged matrices. Also, the errors in the computed matrices A_1 and A_2 are not really independent.

We have shown empirically that, indeed, the accuracy of the Optimized TRIAD is better than that of TRIAD even when the latter uses the vector measured most accurately as the anchor. Note though that in this statement we refer to the average performance; that is, occasionally TRIAD may yield results that are better than those obtained using Optimized TRIAD, but on the average, Optimized TRIAD performs better. Similar to a Kalman filter, the proper blending of the better with the worse TRIAD-generated attitude matrices yields, on the average, a result that is more accurate than the better of the two TRIAD solutions.

Acknowledgment

This work was performed while Itzhack Y. Bar-Itzhack was on a National Research Council–NASA Goddard Space Flight Center Research Associateship.

References

[1]Black, H. D., "A Passive System for Determining the Attitude of a Satellite," *AIAA Journal*, Vol. 2, No. 7, 1964, pp. 1350, 1351.

[2]Shuster, M. D., and Oh, S. D., "Three-Axis Attitude Determination from Vector Observations," *Journal of Guidance and Control*, Vol. 4, No. 1, 1981, pp. 70–77.

[3]Gelb, A. (ed.), *Applied Optimal Estimation*, MIT Press, Cambridge, MA, 1988, pp. 5, 6.

[4]Bar-Itzhack, I. Y., and Meyer, J., "On the Convergence of Iterative Orthogonalization Processes," *IEEE Transactions on Aerospace and Electronic Systems*, Vol. AES-12, No. 2, 1976, pp. 146–151.

Characterization of Ring Laser Gyro Performance Using the Allan Variance Method

Lawrence C. Ng*
Lawrence Livermore National Laboratory, Livermore, California 94511
and
Darryll J. Pines†
University of Maryland, College Park, Maryland 20742-3015

Introduction

THE ring laser gyro (RLG) has become a common instrument in strapdown inertial navigation systems for spacecraft and other aerospace systems. Current RLGs can sense angular rates as low as 0.001 deg/h. The RLG's ability to measure angular rate has several limitations including lock-in, stability, linearity and alignment errors. These limitations contribute to the static noise statistics of the gyro. Static characterization of RLG performance has received much attention since its inception.[1] Performance tests on the RLG have revealed many error sources, such as 1) angle random walk, 2) quantization, 3) bias instability, 4) rate angle walk, 5) rate ramp, 6) sinusoidal component, and 7) scale factor nonlinearity. The first three error terms are normally included as part of the overall performance specifications of an RLG given by the manufacturer. However, traditional approaches such as computing the sampled mean and variance from a measurement set do not reveal the latter five error sources. Although computations of the autocorrelation function or the power spectral density (PSD) distribution do contain a complete description of the error sources, these results are difficult to interpret or extract.

This Engineering Note describes the Allan variance method and its application to the characterization of an RLG's performance[2] under quasisteady state conditions. The method was initially developed by David Allan of the National Bureau of Standards to quantify the error statistics of a cesium beam frequency standard employed by the U.S. Frequency Standards in the 1960s.[3] In general, the method can be applied to analyze the error characteristics of any precision measurement instrument. The key attribute of the method is that it allows for a finer, easier characterization and identification of error sources and their contribution to the overall noise statistics. This Engineering Note presents an overview of the cluster analysis method,[4] explains the relationship between Allan variance and PSD distribution of underlying noise sources, and describes the batch and recursive implementation approaches.

Method of Cluster Analysis

Let angular rate data ω be taken at a rate of f_s samples per second; then from a collection of N data points, we form $K = N/M$ clusters, where M is the number of samples per cluster. The second step is to compute the average for each cluster from the expression

$$\varpi_k(M) = \frac{1}{M}\sum_{i=1}^{M} \omega_{(k-1)M+i}, \qquad k = 1, \ldots, K \tag{1}$$

Received July 26, 1996; revision received Sept. 17, 1996; accepted for publication Sept. 18, 1996. This paper is declared a work of the U.S. Government and is not subject to copyright protection in the United States.

*Member, Technical Staff, Electrical Engineering Division.

†Assistant Professor, Department of Aerospace Engineering. Senior Member AIAA.

The third step is to compute the Allan variance from the cluster averages as follows:

$$\sigma_A^2(\tau_M) \equiv \frac{1}{2}\left\langle [\varpi_{k+1}(M) - \varpi_k(M)]^2 \right\rangle$$

$$\cong \frac{1}{2(K-1)} \sum_{k=1}^{K-1} [\varpi_{k+1}(M) - \varpi_k(M)]^2 \qquad (2)$$

where $\langle\ \rangle$ denotes the ensemble average and $\tau_M = M/f_s$ is the specified correlation time. Note that in Eq. (2) we indicated that the ensemble average is to be computed by the time average. Also note that the expression for the Allan variance comes from the fact that for any two given cluster averages such as ϖ_1 and ϖ_2, the two-point, unbiased, variance estimate is given by

$$\sigma^2 = (\varpi_1 - AVG)^2 + (\varpi_2 - AVG)^2$$

$$= \tfrac{1}{2}(\varpi_2 - \varpi_1)^2 \qquad (3)$$

where $AVG = (\varpi_1 + \varpi_2)/2$ is the two-sample average. The accuracy in the estimate of the root Allan variance increases with additional number of cluster averages. In general the 1-σ accuracy of the computation for K cluster averages is given by

$$\%\text{error} = \frac{100}{\sqrt{2(K-1)}} \qquad (4)$$

Batch Implementation

The batch implementation follows directly from the Allan cluster averages and variances computations given in Eqs. (1) and (2). However, an actual implementation may require segmenting the data into smaller data sets because of limitations in computer array size. When this happens additional work is needed to piece the segmented results together.

Recursive Implementation

A recursive implementation requires recasting Eqs. (1) and (2) into a recursive form. The resulting two recursion equations are called rate recursion and cluster recursion and are summarized in Eqs. (5) and (6), respectively. For the kth cluster of length M, the recursive formulation of Eq. (1) can be written as

$$\varpi_k(m) = [(m-1)/m]\varpi_k(m-1) + [1/M]\omega_{(k-1)M+m}$$

$$m = 1, \ldots, M, \qquad k = 1, \ldots, K \qquad (5)$$

Also for the kth cluster and correlation length m, the recursive formulation of Eq. (2) can be written as

$$\sigma_k^2(m) = \left[\frac{k-2}{k-1}\right]\sigma_{k-1}^2(m) + \left[\frac{1}{2(k-1)}\right](\varpi_k - \varpi_{k-1})$$

$$m = 1, \ldots, M, \qquad k = 1, 2, \ldots \qquad (6)$$

Note that this eliminates the potential limitation from computer array size because for each rate measurement, the average rate is computed sequentially. When the cumulative average rate reaches correlation length m, the mth cluster is updated accordingly. The square root of each cluster recursion output yields the root Allan variance.

Error Source Analysis

The most attractive feature of Allan variance is its ability to sort out various error components by the slopes on the root Allan variance plot provided the different error mechanisms are reasonably separated in the frequency and time domain. In this section we will further clarify the relation of Allan variance and noise source characterization. The key for developing these important relations is found in the relation of Allan variance expressed in the frequency domain as follows:

$$\sigma^2(\tau) = \frac{1}{2}\langle \varpi_{k+1} - \varpi_k \rangle^2 = 4\int_0^\infty \mathrm{d}f\, S_\omega(f) \frac{\sin^4(\pi f \tau)}{(\pi f \tau)^2} \qquad (7)$$

where τ is the cluster correlation time and $S_\omega(f)$ is the PSD of an inertial measurement unit's measured rate information. Using Eq. (7) one can show that the computed Allan variance of different error sources can be expressed in various powers of correlation time.

Quantization Noise

This noise is strictly due to the discrete/quantized nature of a sensor's output. The readout electronics of a device are in terms of counts. The quantization noise represents the minimum resolution level of the sensor. The PSD for such a process, given in Ref. 5, is

$$S_\theta(f) = \tau Q^2 \left(\frac{\sin(\pi f \tau)}{\pi f \tau}\right)^2$$

$$= \tau Q^2 \qquad \text{for} \qquad f < \frac{1}{2\tau} \qquad (8)$$

where Q is the quantization noise coefficient. Its theoretical limit is equal to $S/\sqrt{12}$, where S is the gyro scale factor, for tests with fixed and uniform sampling times. The rate PSD is related to the angle PSD (by a differentiation process) through the equation

$$S_\omega(f) = (2\pi f)^2 S_\theta(f) \qquad (9)$$

and is

$$S_\omega(f) = (4Q^2/\tau)\sin^2(\pi f \tau)$$

$$= (2\pi f)^2 Q^2 \tau \qquad \text{for} \qquad f < 1/2\tau \qquad (10)$$

Substituting Eq. (10) into (7) and performing the integration yields

$$\sigma_Q^2(\tau) = 3Q^2/\tau^2 \qquad (11)$$

Therefore, the root Allan variance of the quantization noise when plotted in a log-log scale is represented by a slope of -1. Note that the root Allan variance is normally expressed in units of degree per hour. Thus, the quantization noise level can be evaluated at any point on the root Allan variance plot where the slope is -1. Also note that quantization noise has a short correlation time or equivalently a wide bandwidth. Because wideband noise can usually be filtered out because of low bandwidth of the vehicle motion in many applications, it is not a major source of error or concern for RLGs.

Angle Random Walk

Angle random walk is a result of integrating a wideband rate PSD noise.[6] Angle random walk due to spontaneous laser emission is a source of error for all RLGs and even more so for RLGs that employ randomized dither as an antilock mechanism.[7] Angle random walk noise is typified by a small varying drift with increasing variance as a function of time. Angle random walk noise typically has a bandwidth less than 10 Hz and is therefore within the bandwidth of most attitude control systems. Thus, angle random walk, if not modeled accurately, can be a major source of error that limits the performance of an attitude control system.

When the input angular rate is small ($\leq$0.2 deg/s), RLGs with two counter-rotating beams tend to experience a lockup phenomenon (i.e., failure to detect nonzero input rate). To avoid this problem, one approach is to dither the RLG assembly with a sinusoidal motion. Furthermore, to avoid the buildup of angular error during each zero rate crossing, the dither amplitude for each half-cycle is randomized. The random zero crossing of the dither signal generates a wideband noise in the rate power spectrum. The associated PSD of the wideband rate noise can be represented by

$$S_\omega(f) = N^2 \qquad (12)$$

where N is the angle random walk coefficient usually expressed in degree per hour per $\sqrt{\text{Hz}}$. Substituting Eq. (12) into Eq. (7) and performing the integration yields

$$\sigma_{\text{arw}}^2(\tau) = N^2/\tau \qquad (13)$$

Note that Eq. (13) indicates that a log-log plot of root Allan variance vs τ has a slope of $-\frac{1}{2}$. Furthermore the numerical value of N can be obtained directly by reading the slope line at $\tau = 1$ h.

Bias Instability

This is the low-frequency bias fluctuations in the measured rate data. The origin of this noise is in the RLG discharge assembly, the electronics, or other components susceptible to random flickering. The rate PSD associated with this noise, also known as $1/f$ noise[8] is

$$S_\omega(f) = \begin{cases} (B^2/2\pi)(1/f), & f \le f_o \\ 0, & f > f_o \end{cases} \tag{14}$$

where B is the bias instability coefficient and f_o is the 3-dB cutoff frequency. Again substituting Eq. (14) into (7) and performing the integration yields

$$\sigma_b^2(\tau) = \frac{2B^2}{\pi}\left[\ell n 2 - \frac{\sin^3(\pi f_o\tau)}{2(\pi f_o\tau)^2}\sin(\pi f_o\tau) + 4\pi f_o\tau\cos(\pi f_o\tau) + C_i(2\pi f_o\tau) - C_i(4\pi f_o\tau)\right]$$

$$= \left(\frac{B}{0.6648}\right)^2 \qquad \text{for} \qquad \tau \gg \frac{1}{f_o} \tag{15}$$

where $C_i(\,)$ is the cosine-integral function. Thus, the bias instability value can be read off the root Allan variance plot at the region where the slope is zero.

Sinusoidal Noise

The PSD of sinusoidal noise is characterized by a number of distinct frequencies. High-frequency noise may originate from plasma oscillations in the laser discharge.[9] A low-frequency source could be the slow motion of the test platform due to periodic environmental changes. A representation of the PSD of this noise containing a single frequency is given as

$$S_\omega(f) = \tfrac{1}{2}\omega_o^2[\delta(f - f_o) + \delta(f + f_o)] \tag{16}$$

where ω_o is the rate amplitude, f_o is the frequency, and $\delta(\,)$ is the Dirac delta function. Substituting Eq. (17) into Eq. (7) and performing the integration yields

$$\sigma_s^2(\tau) = \omega_o^2\left(\frac{\sin^2\pi f_o\tau}{\pi f_o\tau}\right)^2 \tag{17}$$

Thus, the root Allan variance of a sinusoid when plotted in log-log scale would indicate sinusoidal behavior with successive peaks attenuated at a slope of -1. This is one case where a conventional PSD plot is superior in identifying the sinusoidal components.

Rate Random Walk

This noise is a result of integrating a wideband acceleration PSD. This is a random process of uncertain origin, possibly a limiting case of an exponentially correlated noise with a very long correlation time. The mechanical gyro, as well as rate biased laser gyros, exhibits this noise term. The rate PSD associated with this noise (from integrating a wideband acceleration spectrum) is

$$S_\omega(f) = (K/2\pi)^2(1/f^2) \tag{18}$$

where K is the rate random walk coefficient. Substitution of Eq. (18) in Eq. (7) and performing the integration yields

$$\sigma_{\text{rrw}}^2(f) = (K^2/3)\tau \tag{19}$$

This indicates that rate random walk is represented by a slope of $+\frac{1}{2}$ on a log-log plot of $\sigma(\tau)$ vs τ, where K is usually in degrees per square hour per $\sqrt{\text{Hz}}$.

Rate Ramp

This is more of a deterministic error rather than a random noise. Its presence in the data may indicate a very slow monotonic change of the RLG intensity persisting over a long period of time. It could also be due to a very small acceleration of the platform in the same direction and persisting over a long period of time (~hours). It appears as a genuine input to the RLG given by

$$\omega(t) = Rt \tag{20}$$

where R is the rate ramp coefficient. By forming and operating on the clusters of data containing an input given by Eq. (20), we obtain

$$\sigma_{rr}^2 = R^2\tau^2/2 \tag{21}$$

This indicates that the rate ramp noise has a slope of $+1$ in the log-log plot of $\sigma(\tau)$ vs τ.

Extraction of Individual Noise Sources from Allan Variance

In general, any number of random noise components may be present in the data, depending on the type of device and the environment in which the data are obtained. If the noise sources are statistically independent, then the computed Allan variance is the sum of the squares of each error type. A method to extract the level of contribution for each component is needed. The relationships of various error sources and Allan variance as already discussed are summarized in Table 1, which also lists the units of the parameters of interest.

Therefore, assuming statistically independent error sources, the Allan variance can be expressed as the sum of the squares of the variances of one or more error sources:

$$\sigma_{\text{total}}^2 = \sigma_Q^2 + \sigma_{\text{arw}}^2 + \sigma_{\text{bias}}^2 + \sigma_{\text{sinusoid}}^2 + \sigma_{\text{rrw}}^2 + \sigma_{rr}^2 \tag{22}$$

with the root Allan variance given by

$$\sigma_A(\tau) = \sqrt{\sigma_{\text{total}}^2} = f(\sigma_Q, \sigma_{\text{arw}}, \sigma_b, \sigma_{\text{sin}}, \sigma_{\text{rrw}}, \sigma_{rr}) = \sum_{n=-2}^{2} A_n\tau^{n/2} \tag{23}$$

where the coefficients A_n are obtained in a least mean squares sense. Assuming that the computed root Allan variance is expressed in degree per hour and τ is in seconds, then the following expressions can be used for the 1-σ measure of quantization noise, angle random walk, and bias instability, respectively:

$$Q = \left(\frac{\pi \times 10^6}{180 \times 3600 \times \sqrt{3}}\right)A_{-2} \qquad N = (A_{-1}/60) \qquad B = (0.6648)A_0 \tag{24}$$

In many instances, and especially for real-time data analysis, a quick approximation that provides an upper bound on the predicted performance can be obtained without using the least mean squares fit approach. This is doable because the noise components tend to

Table 1 Summary of relation between Allan variance and different error sources

Noise types	Parameter of interest	Units	Root Allan variance, deg/h
Quantization	Q	μrad	$\sigma_Q = \sqrt{3}Q/\tau$
Angle random walk	N	deg/$\sqrt{\text{h}}$	$\sigma_{\text{arw}} = N/\sqrt{\tau}$
Bias instability	B	deg/h	$\sigma_b = \dfrac{B}{0.6648}$
Sinusoidal	ω_o	deg/h	$\sigma_s = \omega_o = \left(\dfrac{\sin^2(\pi f_o\tau)}{\pi f_o\tau}\right)$
Rate random walk	K	(deg/h)/$\sqrt{\text{h}}$	$\sigma_{\text{rrw}} = K\sqrt{(\tau/3)}$
Rate ramp	R	(deg/h/h)	$\sigma_{rr} = R\tau/\sqrt{2}$

Table 2 Accuracy of approximate calculation

Error type	True value	Estimated bound	Error, %
Q	10 μrad	11.72 μrad	17
N	0.1 deg/$\sqrt{}$h	0.18 deg/$\sqrt{}$h	80
B	1 deg/h	1.4 deg/h	40

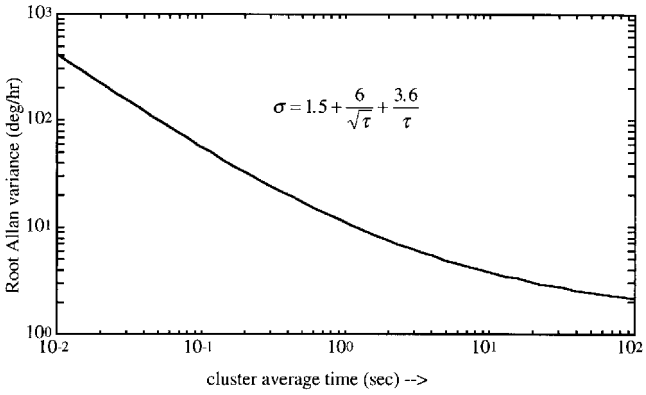

Fig. 1 Typical root Allan variance plot with only quantization, angle random walk, and bias instability.

dominate at different correlation time intervals. For example, let the triplet $\{\tau q, \tau n, \tau b\}$ represent the time on the root Allan variance vs τ plot, where the parameters Q, N, and B are to be evaluated. Then the expression that can quickly bound the values of these parameters are

$$Q = \left(\frac{\pi \times 10^6}{180 \times 3600 \times \sqrt{3}}\right)\sigma_A(\tau_q)\tau_q \tag{25}$$

$$N = \left(\frac{\sigma_A(\tau_n)\sqrt{\tau_n}}{60}\right) \tag{26}$$

$$B = (0.6648)\sigma_A(\tau_b) \tag{27}$$

Assuming a typical set of parameters for the RLG (say, $Q = 10\,\mu$rad, $N = 0.1$ deg/$\sqrt{}$h, and $B = 1$ deg), a corresponding root Allan variance plot is shown in Fig. 1, obtained from solving for the coefficients A_k for $k = \{-2, -1, 0\}$ as given in Eq. (24). Note that we have neglected to include all other noise components except that of quantization, angle random walk, and bias instability. Table 2 summarizes the accuracy in using the approximated expressions as given in Eq. (25). For the typical set of parameters we have chosen for the RLG, the approximate calculations bound the quantization noise by 20%, angle random walk by 80%, and bias instability by 40%. Thus for a more precise estimate of an RLG performance, a complete root Allan variance vs correlation time plot should be generated (may take several hours of actual data recording). Then appropriate noise components can be identified by measuring varying slopes of the plot. A least mean squares fit procedure may then be applied to extract the various components.

Summary and Conclusions

This Engineering Note has summarized the method of Allan variance for analyzing the performance of ring laser gyros in terms of various error sources. These included quantization noise, angle random walk, bias instability, sinusoidal, rate random walk, and rate ramp. We presented two numerical approaches to compute Allan variance: batch implementation and recursive implementation. We have also demonstrated how various error sources can be extracted from the Allan variance computation.

Acknowledgments

This work was supported by the Raptor/Talon program in O-Division, with Program Manager Nick Colella and Talon Systems Engineer Mark Summers. The authors wish to thank the technical staff at Lawrence Livermore National Laboratory for their cooperation and collaboration in making this effort successful.

References

[1] Macek, W. M., and Davis, D. T. M., Jr., "Rotation Rate Sensing with Traveling-Wave Ring Lasers," *Applied Physics Letters*, Vol. 2, 1966, pp. 67, 68.

[2] Anon., "IEEE Specification Format Guide and Test Procedure for Single-Axis Laser Gyros (ANSI)," IEEE Standards Publ. 647-1981, Inst. of Electrical and Electronics Engineers, New York, 1981.

[3] Allan, D. W., "Statistics of Atomic Frequency Standards," *Proceedings of the IEEE*, Vol. 54, No. 2, 1966, pp. 221–230.

[4] Tehrani, M. M., "Ring Laser Gyro Data Analysis with Cluster Sampling Technique," *Proceedings of the SPIE*, Vol. 412, 1983, pp. 207–222.

[5] Papoulis, A., *Probability, Random Variables, and Stochastic Processes*, 3rd ed., McGraw–Hill, New York, 1991, p. 246.

[6] Killpatrick, J., "The Laser Gyro," *IEEE Spectrum*, Oct. 1967, pp. 44–55.

[7] Halford, D., "A General Mechanical Model for $|f|^{\alpha}$ Spectral Density Random Noise with Special Reference to Flicker Noise $1/|f|$," *Proceedings of the IEEE*, Vol. 56, No. 3, 1968, pp. 251–258.

[8] Pasik, D. J., and Gneses, M. I., "A Ring Laser Gyro Strapdown Inertial Navigation System: Performance Analysis and Test Results," AIAA Paper 75-1095, Aug. 1975.

[9] Savage, P. G., "Laser Gyros in Strapdown Inertial Navigation Systems," *Strapdown Inertial Navigation Lecture Notes*, Strapdown Associates, Maple Plain, MN, 1990.